PAPER

Robotic Models for Studying Undulatory Locomotion in Fishes

AUTHORS

George V. Lauder
Jeanette Lim
Ryan Shelton
Museum of Comparative Zoology, Harvard University

Chuck Witt
Erik Anderson
Department of Mechanical Engineering, Grove City College

James L. Tangorra
Department of Mechanical Engineering, Drexel University

ABSTRACT

Many fish swim using body undulations to generate thrust and maneuver in three dimensions. The pattern of body bending during steady rectilinear locomotion has similar general characteristics in many fishes and involves a wave of increasing amplitude passing from the head region toward the tail. While great progress has been made in understanding the mechanics of undulatory propulsion in fishes, the inability to control and precisely alter individual parameters such as oscillation frequency, body shape, and body stiffness, and the difficulty of measuring forces on freely swimming fishes have greatly hampered our ability to understand the fundamental mechanics of the undulatory mode of locomotion in aquatic systems. In this paper, we present the use of a robotic flapping foil apparatus that allows these parameters to be individually altered and forces measured on self-propelling flapping flexible foils that produce a wave-like motion very similar to that of freely swimming fishes. We use this robotic device to explore the effects of changing swimming speed, foil length, and foil-trailing edge shape on locomotor hydrodynamics, the cost of transport, and the shape of the undulating foil during locomotion. We also examine the passive swimming capabilities of a freshly dead fish body. Finally, we model fin-fin interactions in fishes using dual-flapping foils and show that thrust can be enhanced under correct conditions of foil phasing and spacing as a result of the downstream foil making use of vortical energy released by the upstream foil.

Keywords: fish, robot, swimming, biomechanics

Introduction

Fish moving through the water are capable of using a variety of locomotor modes. Some species swim nearly exclusively using their fins and generate propulsive and maneuvering forces using midline fins (dorsal and anal) or paired fins (pectoral and pelvic) (Drucker & Lauder, 1999, 2001; Hove et al., 2001; Standen, 2008; Standen & Lauder, 2007). Other species generate thrust primarily by activating body musculature to bend the body and generate waves passing from the head toward the tail (Gillis, 1996; Jayne & Lauder, 1994, 1995c; Lauder & Tytell, 2006; Rome et al., 1993). The caudal or tail fin is generally considered as an extension of the body in most analyses of fish locomotion, but the tail also possesses a substantial array of intrinsic muscles that appear to stiffen the tail during steady forward swimming and generate a variety of complex tail conformations during maneuvering (Flammang & Lauder, 2008; Flammang & Lauder, 2009).

Despite the large number of studies of fish undulatory locomotion over the last 20 years, there are still many unanswered questions about how the pattern of body deformation is generated, the effect of body stiffness on locomotor performance, what effect different tail shapes have on locomotor function, and how hydrodynamic interactions among different fins might influence the generation of swimming forces. Studies of freely swimming fishes have contributed enormously to our understanding of the mechanics of aquatic locomotion, but such an approach is necessarily limited to the behaviors voluntarily executed by living fishes. And measuring locomotor forces on freely swimming fishes is a challenging proposition. Furthermore, a wide array of interesting experimental manipulations, including changing the flexural stiffness of the body, altering the shape of the tail, and changing the spacing between fins, are clearly impossible to conduct in living animals.

Robotics offers a complementary approach to studies of living fishes by allowing manipulation of variety of parameters such as flexural stiffness, aspect ratio, tail shape, and spacing between adjacent fins. A simple robotic flapping foil device can be used to generate undulatory locomotion in flexible fish-like materials, and forces can

be measured and the effect of changes in body length, stiffness and tail shape can be quantified.

The focus of this paper will be on undulatory locomotion in the water and the use of a robotic flapping apparatus to produce swimming in both flexible plastic foils and a passive freshly dead fish body. After a brief overview of undulatory locomotion in fishes, we discuss the design of a robotic controller for flapping flexible foils that allows measurement of self-propelled speeds (SPS), forces, and torques and the cost of transport associated with foils of different shapes and stiffnesses. In addition, we address an important technical issue in studies of aquatic propulsion: the effect of swimming at non-SPS on body waveform, patterns of force production and wake flow patterns. Finally, we present data on the swimming performance of passive fish bodies and discuss the future for studies of robotically controlled undulatory locomotion. Our overall aim is to introduce a number of case studies with data that show the utility of this approach for studying underwater propulsion and to present an overview of how such studies can provide new ideas and tests for current views of how fish swim.

Overview of Undulatory Propulsion in Fishes

When fish swim using their bodies and tail fin as the primary thrust generators, they pass a wave of bending down the body that increases in amplitude from the head toward the tail (Donley & Dickson, 2000; Gillis, 1996; Jayne & Lauder, 1995a, 1995b; Liao, 2002; Long et al., 1994). This bending wave is produced by a wave of muscular activity that also moves posteriorly and is created by spinal cord and hindbrain pattern generators (Bone et al., 1978; Fetcho & Svoboda, 1993; Fetcho, 1986; Shadwick & Gemballa, 2006). Muscular power to generate thrust is produced primarily by the segmented myotomal musculature in the posterior region of fish, especially during slow swimming (Johnson et al., 1994; Rome et al., 1993; Syme, 2006), and as speed increases more anterior body muscles are recruited to power locomotion. The division of the segmented body musculature into superficial "red" fibers and deeper and more complexly arranged "white" fibers also plays an important role in understanding the multiple "gaits" used by fishes; the relative roles of these two types of muscle fibers can change dramatically as fish change swimming speed and execute rapid locomotor behaviors such as fast-start escapes (Jayne & Lauder, 1993; Tytell & Lauder, 2002).

When fish swim slowly using body undulations, oscillation of the front third or so of the body is quite small even in species as diverse as eels, trout, and tuna (Donley & Dickson, 2000; Gillis, 1998; Lauder & Tytell, 2006), and a primary role of this reduced oscillation appears to be drag reduction by minimizing the frontal area of the fish that encounters oncoming flow. As swimming speed increases, the front region of fish shows increasingly large side-to-side oscillations, which is in part a reflection of the recruitment of body musculature in this more anterior region of the fish.

Even when fish swim by undulatory propulsion using the production of traveling waves, other fins often are used too, and it is incorrect to suggest that fish locomotor modes represent completely distinct patterns of motion. For example, when trout or bluegill sunfish swim using body undulations, they are also actively using their dorsal and anal fins, which play a key role in balancing roll torques and generating thrust (Drucker & Lauder, 2001, 2005; Standen & Lauder, 2005, 2007). In addition, the pelvic fins play an important role in controlling body stability during locomotion in fishes (Harris, 1936, 1938; Standen, 2008, 2010). Fishes also vary in tail shape, and the distinction between the externally symmetrical (homocercal) tail of teleost fishes and the asymmetrical tail in sharks and fish such as sturgeon (Lauder, 1989, 2000) is well known. The heterocercal tail shape induces torques around the body center of mass that requires compensatory changes in body position to allow steady horizontal swimming (Liao & Lauder, 2000; Wilga & Lauder, 2002, 2004b).

Although considerable progress has been made in studies of fish locomotion by investigating the kinematics, muscle activity, and hydrodynamics of live fishes swimming steadily and maneuvering, there are many limits to studies of this kind. Perhaps the two greatest limitations to research on live fishes are (1) the considerable difficulty in measuring locomotor forces and torques produced by the bending body as fish swim freely and (2) the inability to manipulate key variables such as body length, aspect ratio, tail shape, and stiffness. Without an ability to alter such key components that govern locomotor dynamics, we will be limited in our understanding of the factors that influence undulatory propulsion in the water.

The purpose of this paper is to present a number of new case studies using a robotic flapping device for generating undulatory locomotion in engineered materials as a means of

better understanding how fish swim and the dynamics of undulatory propulsion. We discuss different examples to show the utility of this approach and how use of simple flexible foils informs studies of fish locomotion and points to new avenues of research.

Simple Robotic Models of Fish Undulatory Locomotion

We have designed a robotic apparatus that produces controlled heave and pitch motions of flapping foils. The most important features of this device are (1) that it can be set up to be self-propelling (allowing locomotion by flapping foils at their natural swimming speed and not only at imposed speeds) and (2) that forces and torques can be measured on flapping foils during self-propelled swimming so that within-cycle patterns of force and torque oscillation can be compared among foils with different shapes and stiffnesses at different swimming speeds. This apparatus was designed with two sets of flapping foils in series in order to be able to model, with foils, the interactions that can occur between fins of fishes that are arranged in series such as the dorsal and anal fins and the tail fin (discussed further in the section on fin-fin interactions below).

A general description of the first generation of this apparatus is presented in Lauder et al. (2007). Briefly, heave and pitch motors and rotary encoders that allow readouts of foil position are mounted on a carriage above a recirculating flow tank. This carriage is supported on low friction air bearings, which allow the carriage to move in response to foil thrust and drag forces generated during flapping motions. The second generation version of this apparatus has an ATI Nano-17 six-axis force/torque sensor mounted on the shaft supporting the foils (Figure 1A). This permits measurement of three forces and three torques during self-propulsion at sample rates that allow quantification of within-cycle patterns of force production even during self-propulsion. In addition, a linear encoder mounted on the carriage allows a readout of carriage position, and this is used by a Labview program to calculate SPS from data generated by a series of swimming tests at a range of speeds. Synchronizing signals from the LabView program controlling the heave and pitch motors are used to trigger data acquisition from the ATI sensor and also to trigger image acquisition from three synchronized Photron high-speed video

FIGURE 1

Images of a variety of flexible foils and freshly dead trout (*Oncorhynchus mykiss*) attached to a robotic flapping foil apparatus (see Lauder et al., 2007, for details on the basic design). (A) Flexible foil actuated at its leading edge in heave and pitch, suspended in a recirculating flow tank. The red arrow points to an ATI Nano-17 6-axis force/torque transducer on the foil shaft. (B, C) Flexible foils with different trailing edge shapes are used to study the effect of tail shape on swimming performance. (D, E, F) Images of a trout held behind the head to allow imposition of heave and pitch motions to study passive body properties. (E) An image from a trout self-propelling under an imposed heave motion; the body waveform produced is very similar to that generated during swimming.

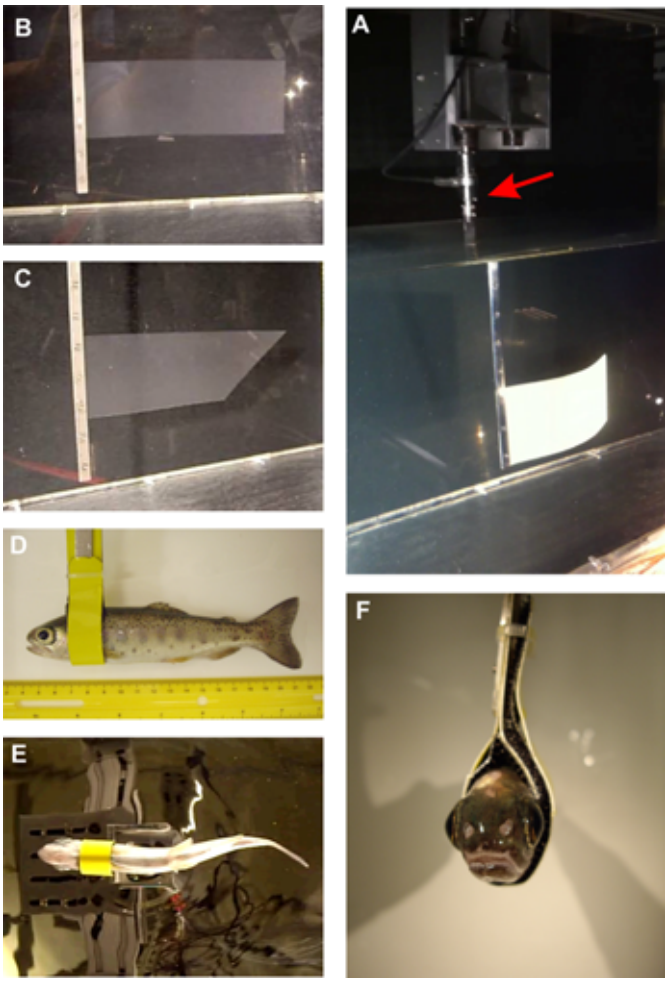

cameras. Images of the flapping foils to quantify both foil motion and hydrodynamic flow patterns are thus synchronized with force and torque measurements on the foil and with the imposed heave and pitch motions on the foil.

The overall goals of using a flapping foil robotic device are to simplify and control as much as possible patterns of motion imposed on flexible and rigid foils that swim through the water and to allow direct testing of the effect on propulsion of a variety of key factors relevant to understanding fish locomotion: tail shape (Figures 1B and 1C), foil flexibility, and interactions among fins. This robotic apparatus can also be used to examine the passive swimming capabilities of a freshly dead fish body (Figures 1D, 1E, and 1F), and below we present data on the ability of fish bodies to passively propel and generate propulsive waveforms under imposed motions. Foils of various kinds are attached to a stainless steel sandwich bar (to hold the leading edge of flexible materials; Figures 1A, 1B, and 1C) to a solid 8-mm shaft (for rigid NACA 0012 foils; see Lauder et al., 2007, and data shown in Figure 11), and flexible fish bodies are mounted in a holder that is attached behind the head (Figures 1D and 1F). Holding systems are designed not to flex in response to imposed heave and pitch motions and to allow forces and torques generated by swimming foils to be transmitted to the force/torque sensor on the shaft. Holding systems such as the sandwich bar system do have their own drag, and this drag is time-dependent due to the heaving and pitching motion of the holding system as the foils self-propel. It is thus not possible to give a single value for the drag of the foil holding system. Since all foil comparisons within a single experimental type used the same holding system and were treated identically, we do not present data on the performance of the holding apparatus alone.

Sample data from a self-propelled flapping foil actuated in heave only are shown in Figure 2. Monitoring foil shaft position and measuring forces in the X (upstream-downstream) and Y (side to side) directions allows calculation of the heave velocity and other derived quantities such as the instantaneous power required by the foil to swim and the coefficients of thrust and power. The cost of transport is calculated by measuring the foil mass and dividing the cost/meter by this value for each foil (see Table 1). Typical peak thrust coefficients for highly flexible foils (flexural stiffness in the range of 10^{-4} to 10^{-6} N m^2) are in the range of ±0.2, lower than typical for rigid foils, but these flexible foils nonetheless are capable of self-propulsion at speeds of 10-30 cm s^{-1}.

A key technical issue arises in studies of flapping foil propulsion that hope to imitate the self-propelled condition achieved by swimming fishes: foils that are not self-propelling may exhibit patterns of thrust oscillation that are not centered around zero. Any foil that is truly self-propelling (and not being dragged through the water at speeds slower or faster than it would naturally move) should generate thrust in an oscillatory pattern, and thrust integrated over a single flapping cycle should equal zero. Graphs in the literature of thrust coefficients during foil-based locomotion that are not centered around zero indicate that the foil was being towed above or below the SPS and do not reflect the self-propelled condition. Data from recordings of foil forces generated during self-propulsion and at speeds below and above the SPS are shown in Figure 3. During self-propelled swimming, the thrust coefficient has a mean of zero over each flapping

FIGURE 2

Sample data from a self-propelling flexible plastic foil (flexural stiffness = 9.2×10^{-5} N m^2) actuated in heave at the leading edge at 2-Hz frequency. Heave position is monitored by rotary encoders, and *X* and *Y* forces are measured by a force transducer mounted on the foil shaft. From the data on foil position, force, and velocity, we make calculations of the instantaneous power, and dimensionless thrust and power coefficients. The dashed lines indicate zero for each trace.

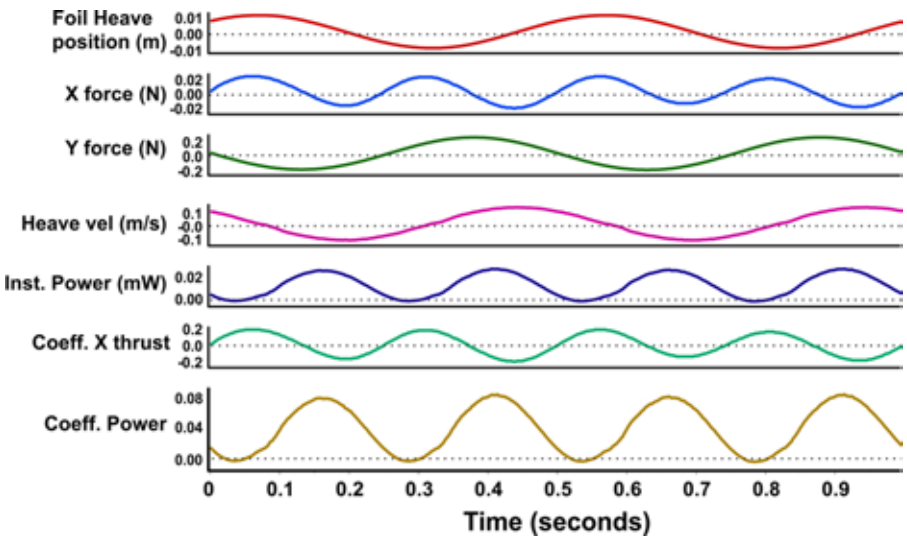

TABLE 1

Locomotor properties of flexible plastic foils of three lengths while self-propelling.

Foil length	SPS (m/s)	Reynolds number	Strouhal number	Work/cycle (mJ)	Cost/meter (mJ/m)	Cost of transport (mJ/g/m)
20	0.105	21,114	0.831	2.248	42.59	106.47
25	0.101	25,250	0.775	2.257	44.69	89.39
35	0.091	31,850	0.349	2.233	49.08	70.11

The three foils were made of the same material with a flexural stiffness of 3.1×10^{-6} N m^2. These highly flexible foils propel at relatively high Strouhal numbers at shorter lengths.
Reynolds and Strouhal numbers are dimensionless.
Foils were actuated at their leading edge with ±1 cm heave, no pitch, at 2 Hz.
Foil span was 6.8 cm for all three foils.
Standard errors for all parameters ranged from 0.3% to 1.5% of the mean values in each column.

cycle. When foils are forced to swim above their SPS, the thrust coefficient curves shift above the zero baseline, and when forced swimming occurs at speeds below the SPS, data are shifted below the baseline.

Change in foil swimming speed above and below the SPS can also have dramatic effects on the kinematics of the foil (Lauder et al., 2011) and on the hydrodynamic wakes displayed by swimming foils. Figure 4 shows the shape observed during swimming of a flexible foil (flexural stiffness, 3.1×10^{-6} N m^2) and the hydrodynamic wakes that result from swimming at, below, and above the average SPS. During swimming at an imposed speed below the SPS, the trailing edge of the foil has a large amplitude and irregular motion that produces a wide bifurcating wake with separate momentum jets to each side (Figure 4A). At the SPS where the foil is allowed to swim freely with no imposed constraints on speed, the foil bends into a regular ribbon-like pattern with a fish-like body wake (see Nauen & Lauder, 2002a, 2002b) and alternating centers of vorticity with a fluid jet that meanders in between these vortical centers (Figure 4B). Above the SPS where the external free-stream flow is increased above SPS and the foil is forced to swim against the increased flow, the foil shape exhibits large amplitude wave-like motion and a substantial drag-like wake with fluid velocities below that of the free stream in the wake (Figure 4C). These changing patterns of foil kinematics and hydrodynamics during swimming that are not under conditions of self-propulsion are most easily seen in highly flexible materials (flexural stiffnesses in the range of 10^{-3} to 10^{-6} N m^2) where the fluid-structure interaction is most evident visually. These flexible materials which have flexural stiffnesses similar to those of fish (McHenry et al., 1995) show fish-like propulsion and deform into wave-like patterns with a fish-like wake (Figure 4B) when allowed to self-propel in a low-friction system.

The structure of the wake behind flapping flexible foils has a significant three-dimensional component due to the finite chord and span, and we

FIGURE 3

Graph showing the dimensionless thrust coefficient versus time for a flexible plastic foil (flexural stiffness = 9.2×10^{-5} N m^2), 20 cm long, 6.8 cm high, actuated in heave ±1 cm at the leading edge at 2-Hz frequency. The red curve shows data for the self-propelled condition (18.8 cm/s), during which the thrust coefficient integrated over a single flapping cycle equals zero. Note that when experiments are done under non-self-propelling conditions (green and blue curves) the plots shift up or down so that the integrated coefficient over a flapping cycle is no longer zero. Data shown have been digitally filtered with a bandpass filter. Strouhal number for this experiment = 0.3 at the SPS (red curve). (Color versions of figures available online at: http://www.ingentaconnect.com/content/mts/mtsj/2011/00000045/00000004.)

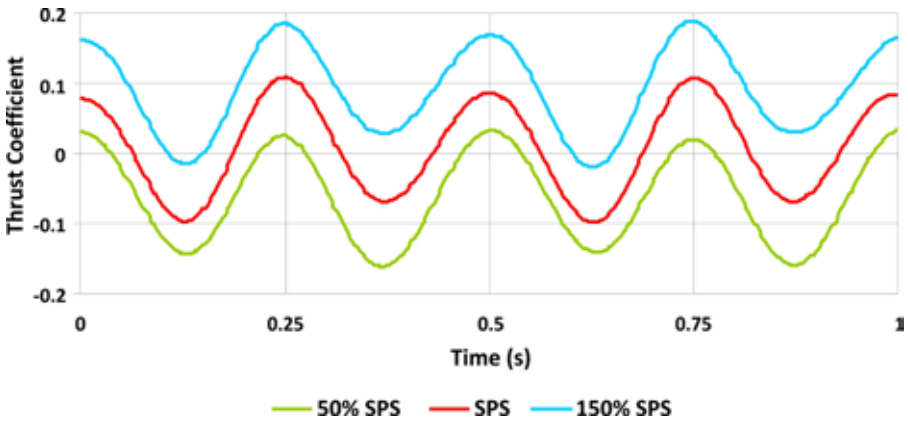

FIGURE 4

Hydrodynamics of propulsion in a flexible foil (flexural stiffness = 3.1×10^{-6} N m^2) swimming below, at, and above its SPS (8.55 cm/s). The foil was actuated at the leading edge with amplitude ±0.5 cm, no pitch, at 3Hz, and is 20 cm long; Strouhal number at the SPS is 0.83 (see Table 1). The bottom margin of the foil is marked in white. Yellow arrows indicate water velocity; red color indicates counterclockwise vorticity; blue color indicates clockwise vorticity. The panels on the left show the whole foil swimming, while the matched panels on the right show a close-in view of the wake structure. The effect of swimming at a non SPS is dramatic, both on foil shape and on wake structure. In (A) the foil swam at an imposed speed of 4.75 cm/s, and in (C) the foil swam at an imposed speed of 25.7 cm/s.

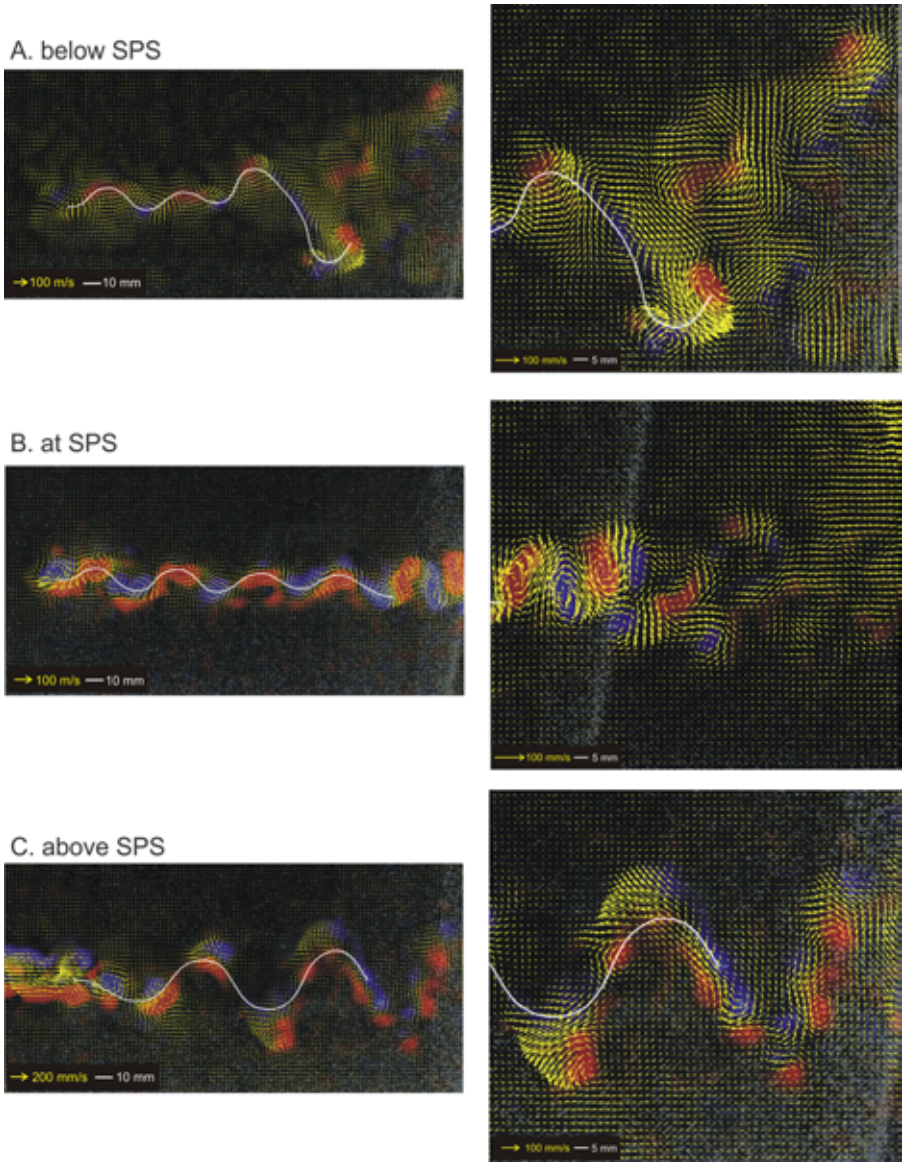

quantified this aspect of foil locomotor dynamics using the volumetric flow visualization system described by Flammang et al. (2011a, 2011b) and Troolin and Longmire (2010). Figure 5 shows how each of the centers of vorticity in the ribbon-like pattern shown in Figure 4B actually represent vortical columns on each side of the foil, which connect to each other above and below the foil. These inter-column connections occur both to upstream and downstream columns on the same side and also across the foil to vortical columns on the opposite side (Figure 5B). To date no other studies have provided three-dimensional wake snapshots during self-propulsion in highly flexible foils, but such studies in the future may reveal interesting patterns of wake interaction among components of the foil and may contribute to explaining the dynamics of propulsion in the flexing bodies.

These results also suggest that at least some of the diversity of fish wakes reported in the literature results from situations in which the fishes were not swimming steadily, either in still water or against imposed flows, as wakes that look like those in Figures 4A and 4C are frequently presented. Fish commonly accelerate and execute small maneuvers during locomotion and considerable effort is needed to ensure that kinematics and wake flow patterns are taken at moments when the fish is swimming steadily. Even small accelerations can substantially change fish wake flows (Tytell, 2004), and data from the flapping foil robot here illustrate that these kinematic and hydrodynamic alterations can be reproduced with flexible foils.

One of the most straightforward questions that could be asked about undulatory propulsion and one that is difficult to study with live fishes is the effect of changing length alone on locomotor performance. We clearly cannot alter fish length experimentally and expect reasonable swimming performance, and comparing fish of different lengths (while useful for studies of scaling) does not account for the many other changes in the musculature and skeleton that occur as fish grow. Table 1 shows data obtained from three flexible foils of different

FIGURE 5

Volumetric flow visualization using the V3V technique (see Flammang et al., 2011a, 2011b) to image the 3D wake structure behind the flexible foil shown in Figure 4B. The trailing edge of the foil is located at the –60 mm position on the *x*-axis, and the fluid structures shown are all in the wake of the foil. This foil was self-propelling and was actuated using the same parameters shown for Figure 4B. (A) The flexible foil achieved a ribbon-like shape and columns of vorticity extend vertically on either side of the foil. Vorticity is isosurfaced at a value of 3.1 (blue surface), and a horizontal slice through the wake is shown to correspond to that shown using 2D piv in Figure 4B (green plane with velocity vectors). (B) The vortical columns on each side of the ribbon-like foil motion connect to each other across the top and bottom of the same side (yellow arrows) and opposite sides (red arrows).

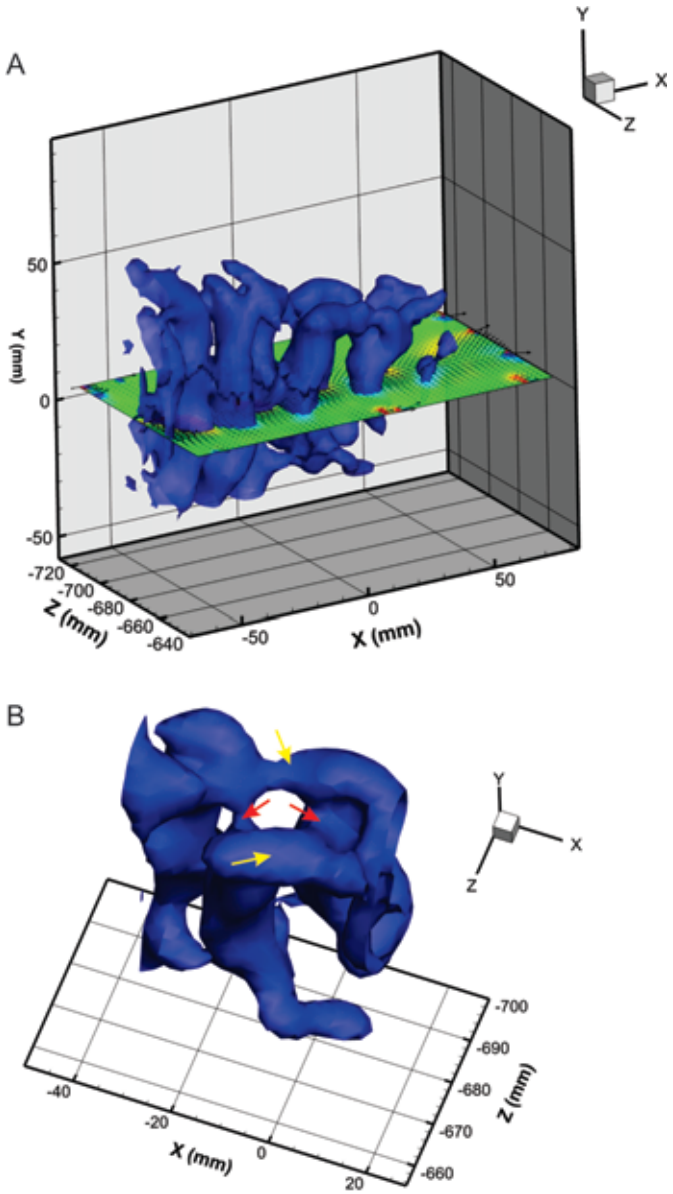

lengths made of the same material and actuated in heave only at the leading edge. Altering the length of this flexible swimming foil from 20 to 35 cm produces only minor changes in the SPS (from 10 to about 9 cm s^{-1}) and hence in Reynolds number but dramatically lowers the Strouhal number (from 0.83 to 0.34; Table 1) due to changes in foil trailing edge amplitude. The work per cycle stays nearly constant, as does the cost per meter (Table 1), but the cost of transport decreases substantially as the increased mass of the longer foils does not result in increased energy requirements for propulsion. Foils such as these that are composed of a very flexible material self-propel at shorter lengths with a Strouhal number that is quite large relative to most self-propelling bodies. At longer lengths, the Strouhal number approaches that of many swimming fishes or rigid foils (Table 1).

Figure 6 shows changes in shape of self-propelling foils made of the same material (flexural stiffness, 3.1 × 10^{-6} N m^2) that occur due to change

FIGURE 6

Graphs to show the effect of length on the shape (amplitude envelope) of a flexible foil (flexural stiffness = 3.1 × 10^{-6} N m^2) swimming at its SPS. This foil was 6.85 cm in chord, and of varying length, given in the color-coded legend. The leading edge was actuated at 2 Hz and with amplitude of ±1 cm. Each plot shows the shape of the foil during self-propulsion as indicated by the peak-to-peak amplitude of the sideways flapping motion. (A, B) Foil shapes as the absolute distance along the foil and as percentage of the total foil length, respectively.

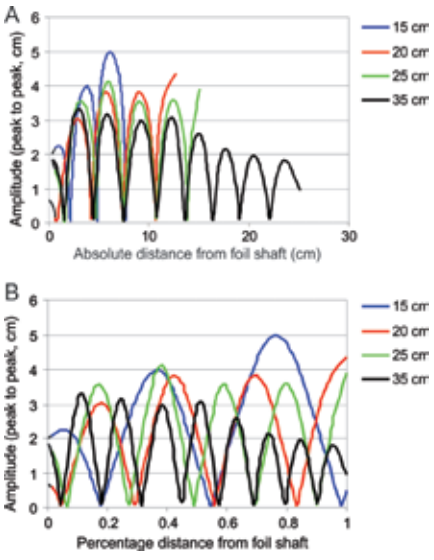

in length. Longer foils show peak excursions at the same locations as shorter foils (Figure 6A) but amplitudes that are lower. Each of the foils of this material generates a ribbon-like shape when self-propelling with a consistent wave-like pattern down its length (see Figure 4B). When the amplitude of each foil as a percentage of foil length is plotted (Figure 6B), changes in amplitude are more evident with side-to-side excursion amplitudes decreasing as length increases while the wave-like pattern is retained. The shortest foils have high amplitudes near the trailing edge and an amplitude envelope that grows along the foil while the longer foils display a tapering amplitude envelope (compare blue and black curves in Figure 6B). These data show that length alone can have significant effects on locomotor efficiency and foil kinematics and that, all other things held constant, foil length increases on the order of 100% can provide reduced costs of transport.

The Effect of Trailing Edge Shape on Swimming Performance

The shape of the trailing tail edge of swimming fishes has been the subject of considerable discussion in the literature, with various authors considering the advantages or disadvantages of fish tails with symmetrical, asymmetrical, or forked shapes (Affleck, 1950; Aleev, 1969; Lauder, 1989; Plaut, 2000; Thomson, 1971, 1976; Wilga & Lauder, 2004a). One advantage of a robotic flapping foil approach is that the trailing edge of a flexible flapping foil can be altered and a variety of configurations constructed that allow the effect of trailing edge shape alone on locomotor performance to be investigated. We designed five different flexible foils (material flexural stiffness = 3.1×10^{-4} N m^2) that control for total length and foil area and allow different tail shapes to be compared for the effect of these changes on swimming speed (Figure 7). Foil 1 corresponds to a highly abstracted "trout-like" body shape with a mostly vertical trailing tail edge, while foils 3 and 4 present a shark-like tail trailing edge shape. Many fish have forked tails, and this shape is represented by foil 5.

FIGURE 7

Propulsion by flexible foils of different shapes (material flexural stiffness = 3.1×10^{-4} N m^2) swimming at their SPS. Each foil was actuated at ±1 cm heave at 2 Hz. Error bars are ±2 SE. Strouhal numbers for these experiments range from 0.2 to 0.3. Foils were constructed to be of differing shapes and areas as follows: foil 1= square trailing edge, area = 131.2 cm^2, dimensions = 6.85 cm × 19.15 cm; foil 2 = angled trailing edge, same length as foil 1, area = 107.71 cm^2; foil 3 = angled trailing edge, same area as foil 1; foil 4 = angled trailing edge: same length and area as foil 1; foil 5 = forked trailing edge: same area as foil 1.

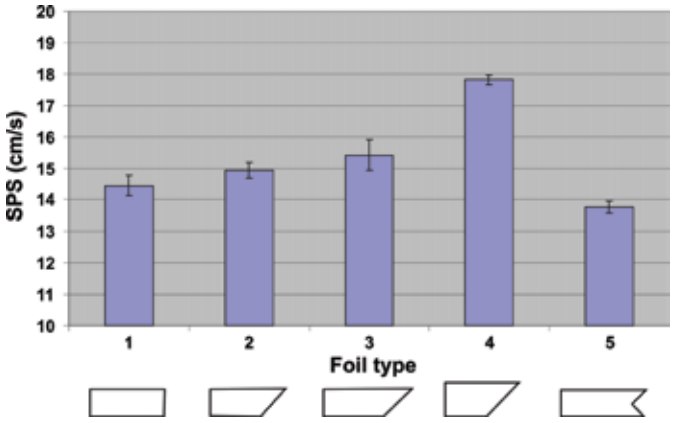

The fastest swimming foil (Figure 7, foil 4) is the one with the most area near the axis of actuation, even though it has the same area as several of the other foils. This result corresponds with our previous results showing that foils with higher aspect ratios and hence more material near the actuator swim significantly faster (Lauder et al., 2011). Interestingly, the foil with the angled trailing edge and the shark tail shape (Figure 7, foil 3) swims significantly faster ($P < 0.003$) than a foil with the same area but a straight trailing edge (Figure 7, foil 1). The foil shape with the significantly lowest swimming speed was the notched shape (Figure 7, foil 5) even though it possesses the same area as foils 1 and 3. The reduced performance of the notched shape may be due to bending of the upper and lower "lobes" of the tail during the flapping motion, and kinematic data obtained for these foils does show that each lobe of this shape twists during the flapping cycle. Twisting of the tail could be reduced by introducing stiffening elements, and this may be one reason that fishes with high-performance tail shapes such as tuna possess substantial stiffening of both the upper and lower tail lobes (Fierstine & Walters, 1968; Westneat & Wainwright, 2001).

Although the angled foil shape swims significantly faster than a foil of the same area with a straight trailing edge (Figure 7: compare foils 1 and 3), more power is required for this foil to swim at this (self-propelled) speed (Figure 8A). The foils were made of

FIGURE 8

Graphs of power consumed (A) and the cost of transport (B) of foils 1 and 3 (see Figure 7) self-propelling. Both foils have the same surface area (131.2 cm^2) and were actuated with ±1 cm heave at 2 Hz. Power values are significantly different at $P = 0.003$. Cost of transport values are not significantly different at $P = 0.07$.

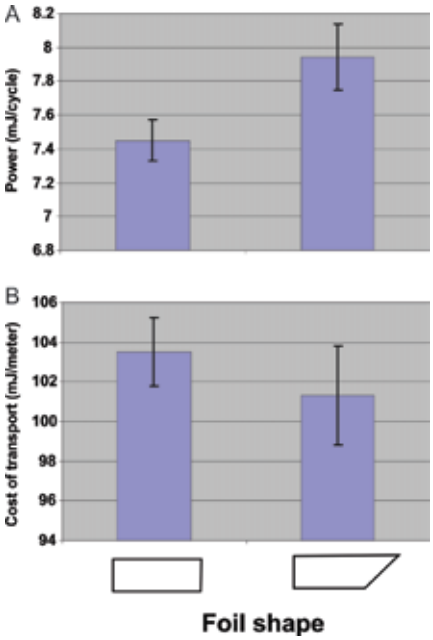

the same material and have the same area, so the cost of transport can be calculated in mJ/m. Figure 8B shows that there is no significant difference ($P = 0.07$) between the foils in cost of transport, although there is a trend in the data toward the angled foil edge costing less per meter resulting in the marginally non-significant difference. Further experiments on both foils will be needed to extend this result and to determine if in fact there is a small difference in cost of transport between these two foil types.

Undulatory Locomotion of a Passive Fish Body

Although flapping flexible foils provide a reasonable and simple model for undulatory propulsion in fishes that minimizes the complexity of the foil and maintains constant material properties along the foil length, fish bodies are clearly different in showing changing material properties from head to tail (McHenry et al., 1995). To better understand the locomotor properties of the passive fish body alone, we used freshly dead rainbow trout (*Oncorhynchus mykiss*) and attached the body to the robotic flapping foil apparatus (Figures 1D, 1E, and 1F). We took care to ensure that rigor mortis had not set in during the experiments and to ensure that the body had thus not stiffened during the time the flapping trials were conducted. By actuating the passive trout body in heave and pitch in various combinations just behind the head, we were able to construct a swimming performance surface for the passive fish body (Figure 9). Body waveforms that are remarkably like those occurring in live trout were generated by the passive fish bodies. These data show that heave amplitude overall has the greater effect on swimming performance than changes in pitch alone. At any given heave value increases in pitch further increase swimming speed, but at higher heave amplitudes near ±2 cm, changes in pitch only produce modest increases in SPS (Figure 9). These data provide an interesting comparison to our previous results showing the effects of heave and pitch actuation on flexible foil propulsion (Lauder et al., 2011). In that study adding pitch motions to baseline heave actuation for foils of varying flexural stiffness did not produce significant increases in foil SPS but did allow stiffer foils to maintain a relatively high swimming speed that would have declined with heave actuation only.

As driving frequency increases, the tail beat amplitude of the passive flapping trout body remains relatively constant from 0.1 to 2.0 Hz before increasing steadily to a peak at 3.5 Hz (Figure 10). These tail beat amplitude values are very similar to those observed in live trout swimming under a variety of locomotor conditions (Liao et al., 2003a; Webb,

FIGURE 9

Performance surface of a freshly dead trout (*Oncorhynchus mykiss*) attached to a robotic controller (see Figures 1D, 1E, 1F) driven at 2 Hz at a variety of heave and pitch amplitudes. This trout was 25.3 cm in total length. The graph shows how SPS of the passive trout body varies with different pitch and heave actuation parameters.

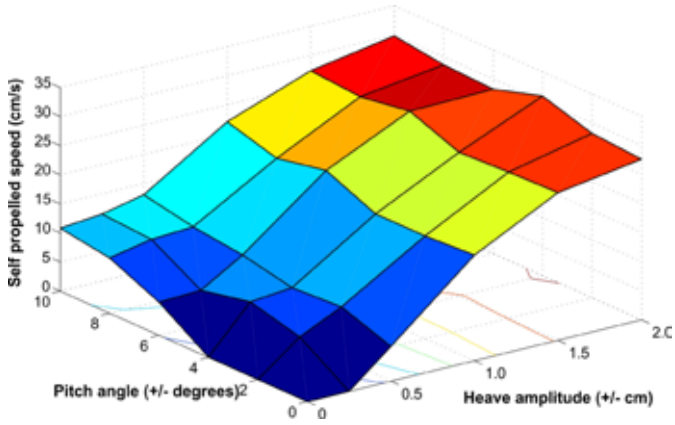

FIGURE 10

Graph of tail-tip amplitude versus heave actuation frequency for a freshly dead trout (*Oncorhynchus mykiss*) attached to a robotic controller driving the passive body at a variety of frequencies. This trout was 25.3 cm in total length and was actuated with a constant heave (±2 cm) and pitch (±5°). Error bars are ±1 SE of the mean.

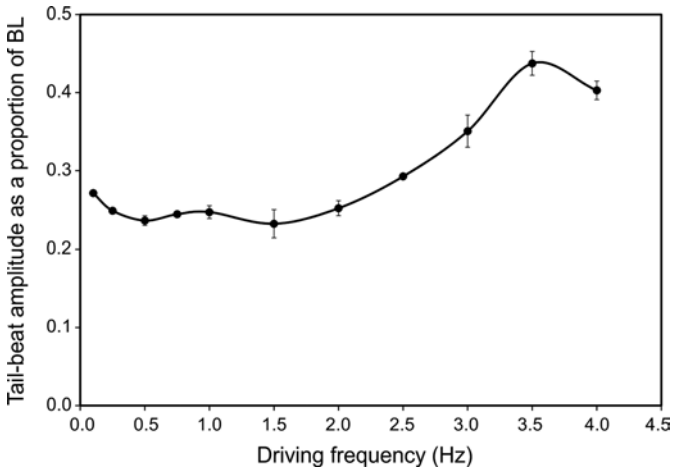

1971; Webb et al., 1984) and increases in tail beat amplitude of the magnitude shown here for the passive trout body are similar to those observed previously as fish increase swimming speed and alter both frequency (primarily) and amplitude (to a lesser extent) of the tail beat.

Although during routine undulatory swimming fish bodies are not passive and are certainly stiffened by body musculature as fish swim, for all but the fastest swimming speeds locomotion is powered by red muscle fibers, which can make up a rather small percentage of body mass (around 1.5% in largemouth bass; see Johnson et al., 1994). The bulk of the locomotor musculature is composed of white fibers that are not activated until the fastest swimming speeds are needed (Jayne & Lauder, 1994, 1995a). Thus, the red muscle fibers can be considered as acting to bend a mostly passive fish body composed of white muscle fibers and associated skeletal tissues that may not be much different in flexural stiffness from the passive bodies studied here.

Also, data on the propulsion of passive fish bodies are relevant to fishes swimming in turbulent flows. Trout swimming in a vortex street have been shown to greatly alter body kinematics and to utilize vortical energy shed from objects in the flow (Liao, 2004; Liao et al., 2003b). The amplitude of the center of mass oscillation by trout swimming in the Karman gait is up to ±2 cm for a 10-cm-long trout, which corresponds on a length-specific basis to the middle region of the performance surface in Figure 9 (Liao et al., 2003a). By greatly reducing muscle activity when trout enter a vortex street, the body becomes largely passive and deforms in response to the oncoming flows. Trouts are able to maintain their position in such flows entirely passively and allow their bodies to extract energy from the oncoming flow and generate thrust. This phenomenon was further demonstrated in a study using passive foils and freshly dead fish bodies to show that the passive trout body alone in a vortex wake can generate sufficient thrust to maintain position in flow (Beal et al., 2006).

Fin-Fin Hydrodynamic Interactions

One of the most intriguing aspects of fish functional design is the arrangement of two fins in series that could allow enhanced locomotor efficiency through hydrodynamic interactions between the fins. For example, the dorsal fin and the anal fin in most fishes are located upstream of the caudal fin, and the wakes shed from these fins could interact with the tail fin during locomotion (Drucker & Lauder, 2001, 2005; Tytell, 2006). Undulatory locomotion using the body also causes the attached median fins to oscillate from side to side, and in the fish species studied so far these fins have been shown also to be actively oscillated by intrinsic fin musculature (Jayne et al., 1996) and thus can generate thrust on their own.

The possibility of fin-fin hydrodynamic interactions during locomotion has been explored in a number of experimental papers on living fishes (Drucker & Lauder, 2001, 2005; Standen, 2008; Standen & Lauder, 2007; Tytell, 2006; Webb & Keyes, 1981) as well as using computational approaches (Akhtar et al., 2007; Weihs et al., 2006). Akhtar et al. (2007) used data on the kinematics of the bluegill dorsal fin and tail from Drucker and Lauder (2001) and performed a two-dimensional computational analysis of the effect of having the fins in series and found that vortex shedding from the dorsal fin can increase thrust of the tail and that the amount of this thrust increase depends on the phasing of dorsal fin and tail motion.

In order to experimentally evaluate hydrodynamic fin-fin interactions using an apparatus in which phasing and the distance between fins can be experimentally manipulated, we used our robotic flapping foil apparatus in the dual-foil configuration with

upstream and downstream foils. Foils were rigid aluminum plates in a NACA 0012 airfoil shape, and each foil could be moved in heave and pitch, and both foils were driven from a common carriage mounted on air bearings as described above. Foils were moved according to the parameters measured for bluegill sunfish dorsal and caudal fins (Drucker & Lauder, 2001) and used by Akhtar et al. (2007) for their computational study of this problem: the upstream foil was moved with heave amplitude of 2.5 cm, the downstream foil at 3.5 cm heave amplitude. Pitch amplitude for both foils was ±20°, and the frequency for both foils was 1.7 Hz, corresponding to the frequency of fin flapping in the bluegill sunfish model case (Drucker & Lauder, 2001).

Increases in SPS as a result of changing foil phase and distance reflect thrust enhancement beyond the thrust achieved by the two foils operating separately (assessed by offsetting the foils from each other so that the downstream foil was no longer in the wake of the upstream foil). A general description of the dual-foil configuration and images of flows around and between the foils are presented in Lauder et al. (2007). Data for SPS were plotted over a range of phase differences between the upstream and downstream foils and polynomial fits to these data points were used to determine the change in SPS with phase (e.g., Figure 11).

Here we present the results of experiments measuring the SPS of dual foil flapping. Figure 11a shows the effect of changing the phase of sinusoidal motion of the downstream foil relative to the upstream foil on SPS for three different spacings between the foils. In each case, there is a clear peak in swimming speed, and as the distance between the foils is increased the peak swimming speed shifts toward a larger phase lag of the downstream foil. Interestingly, the maximal swimming speed of the two foils together does not change significantly as the distance between foils changes, and alterations in phasing between the foils can thus be used to compensate for changes in spacing. For each interfoil spacing, however, there are phase relationships that significantly reduce swimming performance, indicating that thrust of the entire two-foil system is sensitive to phase relationships between two foils flapping. These data correspond very well to the computational results of Akhtar et al. (2007), which showed peak thrust enhancement at a phase

FIGURE 11

Robotic model of fish fin hydrodynamic interactions. Dual NACA 0012 flapping foils in series are driven by a robotic flapping foil apparatus. Details of this device and of the experimental setup are given in Lauder et al. (2007). (A) SPS plotted against the phase difference between the upstream and downstream foils. Foils were arranged with 0 side-to-side offset (in cm) and are thus moving in line with each other with the downstream foil at varying chord length separations from the upstream foil: 0.5, 1, and 2 chord lengths separation; foil chord length was 6.85 cm. Further experimental details are provided in the text. (B) Effect of changing the foil offsets (in cm) so that the downstream foil is not moving in the direct wake of the upstream foil. The one chord length spacing with zero offset curve (dark blue) is the same as in panel (A) and is shown for reference. The other three plots show the effect of a 3.5 cm offset of the midline motion of the downstream foil relative to the upstream foil, removing it from the upstream foil wake.

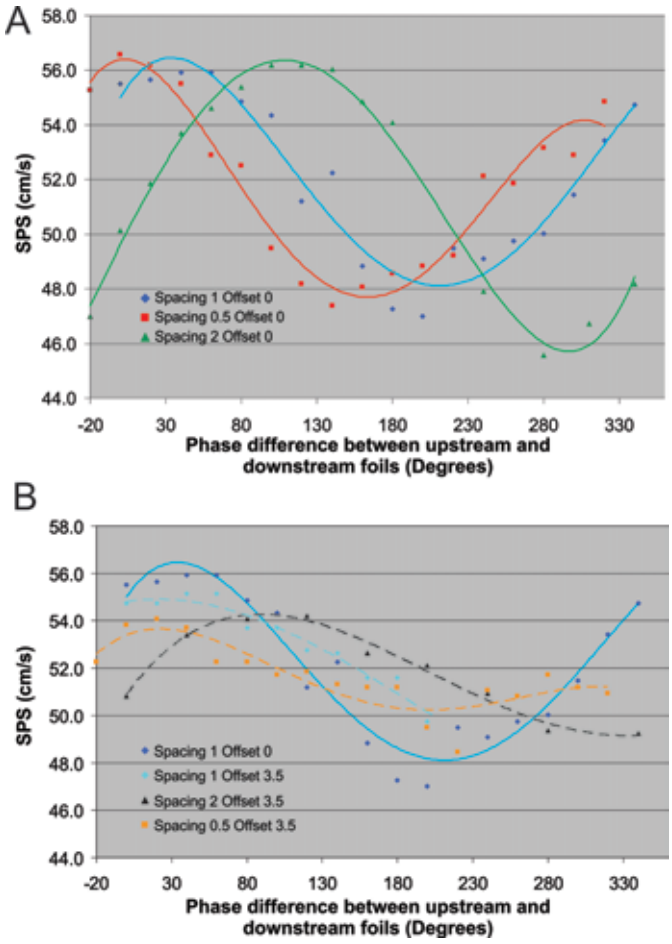

of about 40°, very similar to our data (Figure 11A, blue curve) where the plateau around the SPS peak includes the 40° value.

Figure 11B illustrates the changes in propulsion that result from moving the downstream foil to the side by an offset of 3.5 cm to move it out of the wake of the upstream foil. This effectively creates a tandem foil configuration in which fluid dynamic interactions between the foils are minimized, although not completely eliminated. Comparison of the three offset curves to the zero offset curve shows that offsetting the foils reduces both the SPS and the effect of foil phasing. Offset plots show reduced effects of foil phasing (with lower maxima and higher minima) and less distinct overall peaks in SPS, showing that the downstream foil was not able to improve swimming speed of the two foils together when removed from the upstream foil wake.

Computational work and preliminary flow visualization (Lauder et al., 2007) data indicate that the behavior of tandem foils can be explained in terms of how the downstream foil interacts with fluid structures generated by the upstream foil. The shifting of the peak SPS with increased spacing of the tandem foils can be explained by the fact that, for larger spacings, the convection of those structures to the downstream foil takes longer. That time, *tc*, is simply the spacing between the foils, *s*, divided by the convection velocity, *Uc*. The increase in phase lag, $\Delta\phi$, needed so that the downstream foil meets the fluid structures at the right time is simply

$$\Delta\phi = 2\pi f \frac{(S_2 - S_1)}{U_c}$$

where f is the frequency of flapping and s_2 and s_1 are two different spacings. If we assume that *Uc* is close to the SPS, this equation estimates the $\Delta\phi$ between the peak SPS well for the three spacings we used. The equation predicts $\Delta\phi$ = 0.648 radians, or 37°, for a spacing difference of 0.5 chord lengths, and 74° for a difference of one chord length. The $\Delta\phi$ from our data are approximately 30°and 75° for the corresponding spacing differences. The nearness of the foils and/or higher convection velocities at the smaller spacings may explain the lower than predicted $\Delta\phi$ for the peaks in SPS in these cases. Overall, the agreement is very good considering that the peaks are somewhat broad and the equation for $\Delta\phi$ is a simplification of the fluid dynamics.

The Future of Undulatory Biorobotics

In this paper, we use a robotic tool for investigating a variety of phenomena relating to undulatory propulsion in fishes and present experimental data that would be difficult if not impossible to obtain from studying live animals. The promise of robotic models for studying the biomechanics of locomotion in fishes has just begun to be realized (Curet et al., 2011; Long et al., 2006, 2010; Tangorra et al., 2010, 2011), and fundamental questions relating to the mechanics of undulatory propulsion remain to be addressed. In particular, key unresolved issues are the extent to which changes in body stiffness during propulsion affect locomotor performance (see Long & Nipper, 1996) and how active modulation of stiffness during an undulatory cycle and across changes in swimming speed are achieved and affect propulsive speed and efficiency.

To address these questions, a new generation of robotic undulatory devices will be needed that allow for controlled modulation of body stiffness and the phasing of stiffness changes with undulatory cycles of compression and tension on the bending fish or foil body. An additional arena that is key to making progress in understanding undulatory mechanics is the ability to perturb the locomotor system to assess how stiffness of the body relates to the ability to recover from perturbations. There have been very few studies of perturbations of undulatory locomotor systems (see Webb, 2004), and yet fishes often swim in challenging hydrodynamic environments in which they are forced to recover from impulsive challenges to their undulatory pattern.

Acknowledgments

This work was supported the Office of Naval Research grant N00014-09-1-0352 on fin neuromechanics monitored by Dr. Thomas McKenna and by the National Science Foundation grant EFRI-0938043. We thank the members of the Lauder and Tangorra labs for many helpful discussions on fish fins and flexible flapping foil propulsion and Nate Jackson for his assistance with the dual-flapping foil experiments. Many thanks to Brooke Flammang, Tyson Strand, and Dan Troolin for assistance with the V3V volumetric flow imaging experiments on the undulating plastic foil.

Lead Author:

George V. Lauder
The Museum of
Comparative Zoology

26 Oxford Street, Harvard University
Cambridge, MA 02138
Email: glauder@oeb.harvard.edu

References

Affleck, R.J. 1950. Some points in the function, development, and evolution of the tail in fishes. Proc Zool Soc Lond. 120:349-68. doi: 10.1111/j.1096-3642.1950.tb00954.x.

Akhtar, I., Mittal, R., Lauder, G.V., & Drucker, E. 2007. Hydrodynamics of a biologically inspired tandem flapping foil configuration. Theor Comp Fluid Dyn. 21:155-70. doi: 10.1007/s00162-007-0045-2.

Aleev, Y.G. 1969. Function and Gross Morphology in Fish. Jerusalem: Keter Press.

Beal, D.N., Hover, F.S., Triantafyllou, M.S., Liao, J., & Lauder, G.V. 2006. Passive propulsion in vortex wakes. J Fluid Mech. 549:385-402. doi: 10.1017/S0022112005007925.

Bone, Q., Kiceniuk, J., & Jones, D.R. 1978. On the role of the different fibre types in fish myotomes at intermediate swimming speeds. Fish Bull. 76:691-9.

Curet, O.M., Patankar, N.A., Lauder, G.V., & MacIver, M.A. 2011. Aquatic manoeuvering with counter-propagating waves: A novel locomotive strategy. J R Soc Interface. 8:1041-50. doi: 10.1098/rsif.2010.0493.

Donley, J., & Dickson, K.A. 2000. Swimming kinematics of juvenile Kawakawa tuna (*Euthynnus affinis*) and chub mackerel (*Scomber japonicus*). J Exp Biol. 203:3103-16.

Drucker, E.G., & Lauder, G.V. 1999. Locomotor forces on a swimming fish: Three-dimensional vortex wake dynamics quantified using digital particle image velocimetry. J Exp Biol. 202:2393-412.

Drucker, E.G., & Lauder, G.V. 2001. Locomotor function of the dorsal fin in teleost fishes: Experimental analysis of wake forces in sunfish. J Exp Biol. 204:2943-58.

Drucker, E.G., & Lauder, G.V. 2005. Locomotor function of the dorsal fin in rainbow trout: Kinematic patterns and hydrodynamic forces. J Exp Biol. 208:4479-94. doi: 10.1242/jeb.01922.

Fetcho, J., & Svoboda, K.R. 1993. Fictive swimming elicited by electrical stimulation of the midbrain in goldfish. J Neurophysiol. 70:764-80.

Fetcho, J.R. 1986. The organization of the motoneurons innervating the axial musculature of vertebrates: I. Goldfish (*Carassius auratus*) and mudpuppies (*Necturus maculosus*). J Comp Neurol. 249:521-50. doi: 10.1002/cne.902490408.

Fierstine, H.L., & Walters, V. 1968. Studies in locomotion and anatomy of scombroid fishes. Mem Southern Calif Acad Sci. 6:1-31.

Flammang, B.E., & Lauder, G.V. 2008. Speed-dependent intrinsic caudal fin muscle recruitment during steady swimming in bluegill sunfish, *Lepomis macrochirus*. J Exp Biol. 211:587-98. doi: 10.1242/jeb.012096.

Flammang, B.E., & Lauder, G.V. 2009. Caudal fin shape modulation and control during acceleration, braking and backing maneuvers in bluegill sunfish, *Lepomis macrochirus*. J Exp Biol. 212:277-86. doi: 10.1242/jeb.021360.

Flammang, B.E., Lauder, G.V., Troolin, D.R., & Strand, T. 2011a. Volumetric imaging of shark tail hydrodynamics reveals a three-dimensional dual-ring vortex wake structure. P Roy Soc B. 278. doi: 10.1098/rspb.2011.0489.

Flammang, B.E., Lauder, G.V., Troolin, D.R., & Strand, T.E. 2011b. Volumetric imaging of fish locomotion. Biol Lett. doi: 10.1098/rsbl.2011.0282.

Gillis, G.B. 1996. Undulatory locomotion in elongate aquatic vertebrates: Anguilliform swimming since Sir. James Gray. Am Zool. 36:656-65.

Gillis, G.B. 1998. Environmental effects on undulatory locomotion in the American eel *Anguilla rostrata*: Kinematics in water and on land. J Exp Biol. 201:949-61.

Harris, J.E. 1936. The role of the fins in the equilibrium of the swimming fish: I. Wind tunnel tests on a model of *Mustelus canis* (Mitchell). J Exp Biol. 13:476-93.

Harris, J.E. 1938. The role of the fins in the equilibrium of the swimming fish: II. The role of the pelvic fins. J Exp Biol. 16:32-47.

Hove, J.R., O'Bryan, L.M., Gordon, M.S., Webb, P.W., & Weihs, D. 2001. Boxfishes (Teleostei: Ostraciidae) as a model system for fishes swimming with many fins: Kinematics. J Exp Biol. 204:1459-71.

Jayne, B.C., & Lauder, G.V. 1993. Red and white muscle activity and kinematics of the escape response of the bluegill sunfish during swimming. J Comp Physiol A. 173:495-508. doi: 10.1007/BF00193522.

Jayne, B.C., & Lauder, G.V. 1994. How swimming fish use slow and fast muscle fibers: Implications for models of vertebrate muscle recruitment. J Comp Physiol A. 175:123-31. doi: 10.1007/BF00217443.

Jayne, B.C., & Lauder, G.V. 1995a. Are muscle fibers within fish myotomes activated synchronously? Patterns of recruitment within deep myomeric musculature during swimming in largemouth bass. J Exp Biol. 198:805-15.

Jayne, B.C., & Lauder, G.V. 1995b. Red muscle motor patterns during steady swimming in largemouth bass: Effects of speed and correlations with axial kinematics. J Exp Biol. 198:1575-87.

Jayne, B.C., & Lauder, G.V. 1995c. Speed effects on midline kinematics during steady undulatory swimming of largemouth bass, *Micropterus salmoides*. J Exp Biol. 198:585-602.

Jayne, B.C., Lozada, A., & Lauder, G.V. 1996. Function of the dorsal fin in bluegill sunfish: Motor patterns during four locomotor behaviors. J Morphol. 228:307-26. doi:10.1002/(SICI)1097-4687(199606)228:3<307::AID-JMOR3>3.0.CO;2-Z.

Johnson, T.P., Syme, D.A., Jayne, B.C., Lauder, G.V., & Bennett, A.F. 1994. Modeling red muscle power output during steady and unsteady swimming in largemouth bass (*Micropterus salmoides*). Am J Physiol. 267:R481-8.

Lauder, G., Madden, P.G.A., Tangorra, J., Anderson, E., & Baker, T.V. 2011. Bioinspiration from fish for smart material design and function. Smart Mater Struct. in press.

Lauder, G.V. 1989. Caudal fin locomotion in ray-finned fishes: Historical and functional analyses. Am Zool. 29:85-102.

Lauder, G.V. 2000. Function of the caudal fin during locomotion in fishes: Kinematics, flow visualization, and evolutionary patterns. Am Zool. 40:101-22. doi: 10.1668/0003-1569(2000)040[0101:FOTCFD]2.0.CO;2.

Lauder, G.V., Anderson, E.J., Tangorra, J., & Madden, P.G.A. 2007. Fish biorobotics: Kinematics and hydrodynamics of self-propulsion. J Exp Biol. 210:2767-80. doi: 10.1242/jeb.000265.

Lauder, G.V., & Tytell, E.D. 2006. Hydrodynamics of undulatory propulsion. In: Fish Biomechanics. Volume 23 in Fish Physiology, eds. Shadwick, R.E., & Lauder, G.V., 425-68. San Diego: Academic Press.

Liao, J. 2002. Swimming in needlefish (Belonidae): Anguilliform locomotion with fins. J Exp Biol. 205:2875-84.

Liao, J. 2004. Neuromuscular control of trout swimming in a vortex street: Implications for energy economy during the Karman gait. J Exp Biol. 207:3495-506. doi: 10.1242/jeb.01125.

Liao, J., Beal, D.N., Lauder, G.V., & Triantafyllou, M.S. 2003a. The Kármán gait: Novel body kinematics of rainbow trout swimming in a vortex street. J Exp Biol. 206:1059-73. doi: 10.1242/jeb.00209.

Liao, J., & Lauder, G.V. 2000. Function of the heterocercal tail in white sturgeon: Flow visualization during steady swimming and vertical maneuvering. J Exp Biol. 203:3585-94.

Liao, J.C., Beal, D.N., Lauder, G.V., & Triantafyllou, M.S. 2003b. Fish exploiting vortices decrease muscle activity. Science. 302:1566-9. doi: 10.1126/science.1088295.

Long, J.H., Jr., Koob, T.J., Irving, K., Combie, K., Engel, V., Livingston, N., … Schumacher, J. 2006. Biomimetic evolutionary analysis: Testing the adaptive value of vertebrate tail stiffness in autonomous swimming robots. J Exp Biol. 209:4732-46. doi: 10.1242/jeb.02559.

Long, J.H., McHenry, M.J., & Boetticher, N.C. 1994. Undulatory swimming: How traveling waves are produced and modulated in sunfish (*Lepomis gibbosus*). J Exp Biol. 192:129-45.

Long, J.H., & Nipper, K.S. 1996. The importance of body stiffness in undulatory propulsion. Am Zool. 36:678-694.

Long, J.H., Porter, M.E., Root, R.G., & Liew, C.W. 2010. Go reconfigure: How fish change shape as they swim and evolve. Integr Comp Biol. 50:1120-39. doi: 10.1093/icb/icq066.

McHenry, M.J., Pell, C.A., & Long, J.A. 1995. Mechanical control of swimming speed: Stiffness and axial wave form in undulating fish models. J Exp Biol. 198:2293-305.

Nauen, J.C., & Lauder, G.V. 2002a. Hydrodynamics of caudal fin locomotion by chub mackerel, *Scomber japonicus* (Scombridae). J Exp Biol. 205:1709-24.

Nauen, J.C., & Lauder, G.V. 2002b. Quantification of the wake of rainbow trout (*Oncorhynchus mykiss*) using three-dimensional stereoscopic digital particle image velocimetry. J Exp Biol. 205:3271-9.

Plaut, I. 2000. Effects of fin size on swimming performance, swimming behavior and routine activity of zebrafish *Danio rerio*. J Exp Biol. 203:813-20.

Rome, L.C., Swank, D., & Corda, D. 1993. How fish power swimming. Science. 261: 340-3. doi: 10.1126/science.8332898.

Shadwick, R., & Gemballa, S. 2006. Structure, kinematics, and muscle dynamics in undulatory swimming. In: Fish Biomechanics. Volume 23 in Fish Physiology, eds. Shadwick, R.E., & Lauder, G.V., 241-280. San Diego: Academic Press.

Standen, E.M. 2008. Pelvic fin locomotor function in fishes: Three-dimensional kinematics in rainbow trout (*Oncorhynchus mykiss*). J Exp Biol. 211:2931-42. doi: 10.1242/jeb.018572.

Standen, E.M. 2010. Muscle activity and hydrodynamic function of pelvic fins in trout (Oncorhynchus mykiss). J Exp Biol. 213:831-41. doi: 10.1242/jeb.033084.

Standen, E.M., & Lauder, G.V. 2005. Dorsal and anal fin function in bluegill sunfish (*Lepomis macrochirus*): Three-dimensional kinematics during propulsion and maneuvering. J Exp Biol. 205:2753-63. doi: 10.1242/jeb.01706.

Standen, E.M., & Lauder, G.V. 2007. Hydrodynamic function of dorsal and anal fins in brook trout (*Salvelinus fontinalis*). J Exp Biol. 210:325-39. doi: 10.1242/jeb.02661.

Syme, D.A. 2006. Functional properties of skeletal muscle. In: Fish Biomechanics. Volume 23 in Fish Physiology, eds. Shadwick, R.E., & Lauder, G.V., 179-240. San Diego: Academic Press.

Tangorra, J., Phelan, C., Esposito, C., & Lauder, G. 2011. Biorobotic models of highly deformable fins for studies of the mechanics and control of fin forces. Integr Comp Biol. in press. doi: 10.1093/icb/icr036.

Tangorra, J.L., Lauder, G.V., Hunter, I., Mittal, R., Madden, P.G., & Bozkurttas, M. 2010. The effect of fin ray flexural rigidity on the propulsive forces generated by a biorobotic fish pectoral fin. J Exp Biol. 213:4043-54. doi: 10.1242/jeb.048017.

Thomson, K.S. 1971. The adaptation and evolution of early fishes. Q Rev Biol. 46: 139-66. doi: 10.1086/406831.

Thomson, K.S. 1976. On the heterocercal tail in sharks. Paleobiology. 2:19-38.

Troolin, D., & Longmire, E. 2010. Volumetric velocity measurements of vortex rings from inclined exits. Exp Fluids. 48:409-20. doi: 10.1007/s00348-009-0745-z.

Tytell, E.D. 2004. Kinematics and hydrodynamics of linear acceleration in eels,

Anguilla rostrata. P Roy Soc Lond B. 271:2535-40. doi: 10.1098/rspb.2004.2901.

Tytell, E.D. 2006. Median fin function in bluegill sunfish, *Lepomis macrochirus*: Streamwise vortex structure during steady swimming. J Exp Biol. 209:1516-34. doi: 10.1242/jeb.02154.

Tytell, E.D., & Lauder, G.V. 2002. The c-start escape response of *Polypterus senegalus*: Bilateral muscle activity and variation during stage 1 and 2. J Exp Biol. 205:2591-603.

Webb, P.W. 1971. The swimming energetics of trout: I. Thrust and power output at cruising speeds. J Exp Biol. 55:489-520.

Webb, P.W. 2004. Response latencies to postural disturbances in three species of teleostean fishes. J Exp Biol. 207:955-61. doi: 10.1242/jeb.00854.

Webb, P.W., & Keyes, R.S. 1981. Division of labor between median fins in swimming dolphin (Pisces: Coryphaenidae). Copeia. 1981:901-04. doi: 10.2307/1444198.

Webb, P.W., Kostecki, P.T., & Stevens, E.D. 1984. The effect of size and swimming speed on the locomotor kinematics of rainbow trout. J Exp Biol. 109:77-95.

Weihs, D., Ringel, M., & Victor, M. 2006. Aerodynamic interactions between adjacent slender bodies. AIAA J. 44:481-4. doi: 10.2514/1.18902.

Westneat, M., & Wainwright, S.A. 2001. Mechanical design for swimming: Muscle, tendon, and bone. In: Tuna: Physiology, Ecology, and Evolution, eds. Block, B., & Stevens, E.D., 271-311. San Diego: Academic Press. doi: 10.1016/S1546-5098(01)19008-4.

Wilga, C.D., & Lauder, G.V. 2002. Function of the heterocercal tail in sharks: Quantitative wake dynamics during steady horizontal swimming and vertical maneuvering. J Exp Biol. 205:2365-74.

Wilga, C.D., & Lauder, G.V. 2004a. Biomechanics of locomotion in sharks, rays and chimeras. In: Biology of Sharks and Their Relatives, eds. Carrier, J.C., Musick, J.A., & Heithaus, M.R., 139-64. Boca Raton: CRC Press.

Wilga, C.D., & Lauder, G.V. 2004b. Hydrodynamic function of the shark's tail. Nature. 430:850. doi: 10.1038/430850a.